

Band structure and charge doping effects of potassium-adsorbed FeSe/SrTiO₃ system

Fawei Zheng,¹ Li-Li Wang,² Qi-Kun Xue,² and Ping Zhang^{1,*}

¹*Institute of Applied Physics and Computational Mathematics, Beijing 100088, China*

²*Department of Physics, Tsinghua University, Beijing 100084, China*

Abstract

We theoretically study, through combining the density functional theory and an unfolding technique, the electronic band structure and the charge doping effects for the deposition of potassium (K) on multilayer FeSe films grown on SrTiO₃ (001) surface. These results form a theoretical base line for further detailed studies of low-temperature electronic properties and their multiway quantum engineering of FeSe thin films. We explain the Fermi surface topology observed in experiment and formulate the amount of doped electrons as a function of atomic K coverage. We show that the atomic K deposition efficiently dopes electrons to top layer FeSe. Both checkerboard and pair-checkerboard antiferromagnetic (AFM) FeSe layers show electron pockets at M point and no Fermi pocket at Γ point with moderate atomic K coverage. The electron transfer from K adsorbate to FeSe film introduces a strong electric field, which leads to a double-Weyl cone structure at M point in the Brillouin zone of checkerboard-AFM FeSe. We demonstrate that with experimentally accessible heavy electron doping, an electron-like Fermi pocket will emerge at Γ point, which should manifest itself in modulating the high-temperature superconductivity of FeSe thin films.

PACS numbers: 74.70.Xa, 68.35.-p, 74.25.Jb

*Corresponding author: zhang_ping@iapcm.ac.cn

The superconductivity in monolayer FeSe film grown on SrTiO₃ (001) surface has recently been observed [1–9]. It is attracting extensive studies on this unique system [10–21]. The monolayer FeSe film is the fundamental building block of crystalline iron-based superconductors. The FeSe/SrTiO₃ system provides us with a nice platform to study the monolayer FeSe film thoroughly, and may shed light on superconducting mechanism of the entire iron-based superconductors. The superconducting transition temperature T_c of FeSe/SrTiO₃ exceeds that of bulk FeSe by one order of magnitude [1, 22–24]. Whereas, further grown FeSe layers on FeSe/SrTiO₃ [25–27] and FeSe layers on graphene [28] and CaF₂ [29] do not show such a high- T_c enhancement, which indicates a critical role played by the interaction between the monolayer FeSe and SrTiO₃ substrate. This interface-induced T_c enhancement is supposed to be closely associated with the electron doping from SrTiO₃ substrate [30–34], as well as with the strength of electron-phonon interaction [1, 35–39]. Angle resolved photoemission spectroscopy (ARPES) measurements have found that there are only electron-like Fermi pockets that locate at M point, while the hole-like Fermi pocket at Γ point disappears [2, 3, 32]. This peculiar Fermi surface topology indicates that the system is strongly electron doped. The amount of doped electrons is increased with increasing annealing time, and finally reaches a saturated value. Recently, by depositing potassium (K) atoms onto multilayer FeSe films grown on SrTiO₃ surface (we henceforth name the system as K/n-FeSe/SrTiO₃, where n is the number of FeSe layers), Miyata *et al.* demonstrated that atomic K deposition can dope electrons to FeSe films more effectively [40]. In this way, the electron doping can be tuned continually and reversely, thus expanding the accessible doping range towards the heavily electron-doped region. The superconducting phase diagram shows a clear dome-like shape and the maximum T_c is as high as 48 Kelvin [40]. Along this line, further experimental measurements are being carried out [41, 42].

To self-consistently depict the above-mentioned charge doping and predict new adsorbate-tuned electronic properties superposed onto the inherently profound physics of the FeSe/SrTiO₃ system, apparently, a systematic and enlightening theoretical study of K deposition affection to the electronic structures of FeSe films is essential but still keeps to be initialized. In this paper, by using the density functional theory (DFT) based first-principles calculations and checkerboard (CB) as well as pair-checkerboard (PCB) antiferromagnetic (AFM) models, the energy band structure and the charge transfer effects of the K/n-FeSe/SrTiO₃ system is studied. The Fermi surface topology observed in experiment is

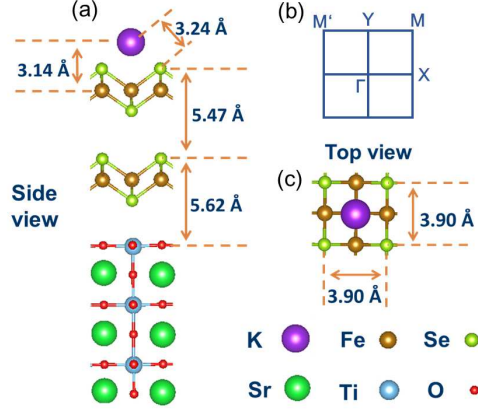


FIG. 1: (Color online) The side (a) and top (c) view of K/2-FeSe/STO atomic structure. Panel (b) shows the two-dimensional first Brillouin zone of K/n-FeSe/STO.

satisfactorily explained. We find that only the top layer FeSe is effectively charged. The amount of doped electrons linearly depends on atomic K coverage (denoted by ρ_K). The induced electric field strongly distorts the CB FeSe energy bands, leading to a double-Weyl cone structure at M point. Remarkably, our results also show that an electron-like Fermi pocket will rapidly develop at Γ point if the amount of doped electrons further increases to be larger than $0.2 e$ per FeSe formula unit in CB FeSe. For PCB FeSe, the critical value is $0.17 e$.

The DFT calculations in this work were mainly performed by using *Vienna Ab-initio Software Package* (VASP) [43]. The atom core electrons were described by projector augmented wave (PAW) method [44, 45]. Perdew-Burke-Ernzerhof [46] (PBE) functional was used to treat the electronic exchange-correlation. The energy cutoff for the plane-wave basis was set at 400 eV. The first Brillouin zone was sampled in the k -space with Monkhorst-Pack scheme and grid sizes are 13×13 , 7×7 , 5×5 and 8×4 for 1×1 , 2×2 , 3×3 and 2×4 supercells, respectively. We have checked that the total energy is converged for the cutoff energy and k -point sampling. The atomic structure was relaxed until the force on each atom is smaller than 0.01 eV/\AA . The K/n-FeSe/SrTiO₃ can be divided into three parts (K atoms, FeSe layers and SrTiO₃ substrate). Considering that weak attractions exist in this composite system, we have added the van der Waals correction [47] to DFT calculations. The slab models were used and more than 12 \AA vacuum space was added to avoid artificial interaction. The in-plane lattice parameter was set to 3.901 \AA [34]. We used 6-layer SrTiO₃ with the TiO₂ layer

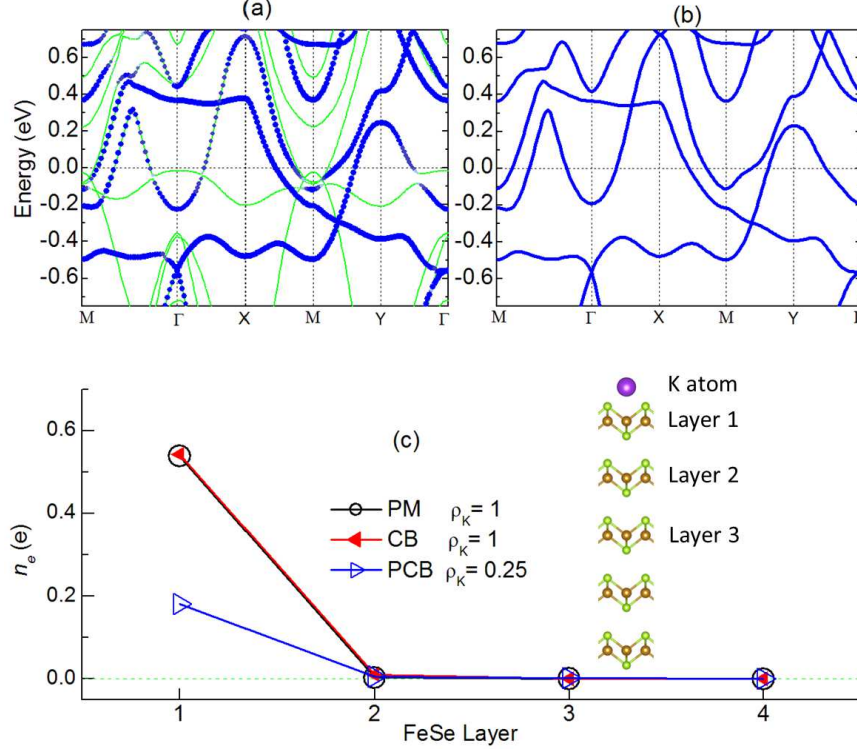


FIG. 2: (Color online) The energy band structures of K/2-FeSe/STO (a) and K/FeSe (b) isolated systems. In panel (a), the energy bands projected to K atom and top layer FeSe are signed by blue dots. The Fermi level is set to be zero. Panel (c) shows the charge transfer from K atom to the top few FeSe layers in a K/n-FeSe system. The inner figure shows the K/n-FeSe atomic structure.

on the top to mimic the SrTiO₃ substrate. Besides the VASP code, we also performed DFT calculations in *Quantum Espresso* (QE) [48] code with norm-conserving pseudopotentials [49] to get accurate unfolded electronic energy bands by using a home-built code.

The relaxed atomic structure of the K/2-FeSe/SrTiO₃ is shown in Figs. 1(a,c). The ρ_K is 1, which is one K atom per FeSe primary cell. The thickness of the down layer FeSe, which is defined by the distance between the top Se atom in FeSe and top layer TiO₂, is 5.62 Å. The thickness of the top layer FeSe is 5.47 Å, which is very close to the c lattice parameter of bulk FeSe [24]. The K atoms adsorb on top layer FeSe, right on the top of bottom Se atoms. The distances between the K atom and top Se atoms and Fe plane are determined to be 3.24 Å and 3.14 Å, respectively.

The energy bands of K/2-FeSe/SrTiO₃ with CB magnetic orientation are shown in Fig. 2(a). All the energy bands are plotted in green color, and the energy bands that are mainly

contributed by top layer FeSe and K atom are signed by blue dots. To compare with these energy bands, we also calculated the energy bands of K/FeSe system, which consists only of the K atoms and top layer FeSe. The resultant band structure is shown in Fig. 2(b). It is quite similar to the blue dots in Fig. 2(a), while the energy bands in Fig. 2(a) without blue dots are quite similar to those in Fig. 2(a) in Ref. [34]. This means that the interaction between FeSe layers is quite weak, and the atomic K adsorption only affects the top layer FeSe. We then further checked the energy bands of K/3-FeSe/SrTiO₃ system with CB magnetic orientation and K/2-FeSe/SrTiO₃ with PCB magnetic orientation. The results are the same by the observed fact that the adsorbed K atoms only influence the top layer FeSe and have negligible effects on the other FeSe layers. The doping charge distribution in a multilayer FeSe system can be calculated by using a K/n-FeSe slab model. The calculation results of K/5-FeSe model with different ρ_K and magnetic orientations are shown in Fig. 2(c). All the calculation results show that the top layer FeSe has much more doping electrons than the second layer (more than 31 times larger). The doping electrons in the non-top layer FeSe is negligible. This phenomenon agrees with the most recent experimental results [50]. In other words, the K/FeSe slab model can approximately describe the K adsorption on n-FeSe/SrTiO₃ ($n \geq 2$) systems correctly. Thus, in this work, we studied the detailed K adsorption effects by using K/FeSe slab model with different values of ρ_K .

We then studied the energy bands of CB FeSe with different ρ_K . The energy bands can be calculated by using a primary cell, if the ρ_K is 0 or 1. The corresponding results are shown in Figs. 3(a,e). For the cases of fractional ρ_K , supercells have to be used to calculate their electronic structures. However, the supercell energy bands are quite different from primary cell energy bands. In order to compare energy bands between the primary cell and the supercell, we resort to unfolding the supercell energy bands by using a home-built code [51]. In PAW calculations, the norm of PAW wavefunction is not restricted to be unity. Therefore, the energy band unfolding weight within PAW is not accurate [51]. Thus, we performed the QE calculations with norm-conserving pseudopotentials to unfold the supercell energy bands accurately. The plane wave cutoff energy was 1490 eV. The k -space samplings were set the same with VASP calculations. We tested that the FeSe and K/FeSe primary cell energy bands calculated by QE agree well with VASP results. After the QE supercell calculations, the *Wannier90* code [52] was used to calculate the maximum localized Wannier functions (MLWFs). We added a few Fortran lines to *Wannier90* to write

out the MLWFs in a format that is easier for further calculations. After that, our *Quantum Unfolding* code [51, 53] reads these MLWFs and unfold the electronic energy bands to the first Brillouin zone of FeSe primary cell.

We used 2×2 CB FeSe supercells with 1, 2 and 3 K atoms adsorbed on one side of FeSe monolayer to mimic the K/n-FeSe/SrTiO₃ systems. The corresponding ρ_K are 0.25, 0.5 and 0.75 respectively. The unfolded energy bands are shown in Figs. 3(b-d). For comparison, the energy bands for the cases of $\rho_K=0$ and $\rho_K=1$ (by usage of 1×1 primary cells) are also displayed in Fig. 3 [panels (a) and (e)]. Initially [panel (a)], the Fermi surface contains two parts. They are a small electron-like Fermi pocket at M point and a hole-like Fermi pocket at Γ point. With increasing ρ_K step by step, then, the energy bands continually go down with respect to the Fermi level. As a consequence, the hole-like Fermi pocket disappears, while the electron pocket enlarges its size dramatically. Remarkably, these Fermi surface transformations shown in Figs. 3(a-c) agree well with the most recent ARPES experiments [40], in which the K depositions with the electron doping up to 0.15 e per FeSe formula unit were explored. Prominently, as we increase ρ_K , a conduction band (indicated by a green arrow) at Γ point lowers its energy much faster than other energy bands. It closes to the Fermi level at $\rho_K = 0.5$, and crosses the Fermi level at $\rho_K = 0.75$. The crossing introduces an electron-like Fermi pocket at Γ point. This agrees with the previous energy band calculation in uniformly electron doped FeSe monolayer [11]. Our unfolded energy bands show that this phenomenon is robust against the doping charge distribution, and may be realized in K/n-FeSe/SrTiO₃ system. It is a Lifshitz transition since the Fermi surface topology is altered. The effect of this Lifshitz transition to FeSe monolayer superconducting is still not clear, therefore need more theoretical and experimental study.

On the other hand, comparing to the case of uniformly electron doped FeSe, the electron doping raised by atomic K adsorption brings about a new feature. That is, the energy bands at M point become non-symmetric, as shown by the red arrows in Fig. 3. They move to the right side (M-Y direction). The bias direction depends on the electron spin. We have checked that the spin-down energy bands bias to the left side (M-X direction). This phenomenon also exists in 1-FeSe/SrTiO₃ system [34]. Our DFT and tight-binding calculations on FeSe monolayer in electric field revealed this peculiar feature, and concluded that the energy bands biased at M point is caused by a strong electric field along the perpendicular direction of FeSe film. It is a self-established electric field as a consequence of charge transfer. The

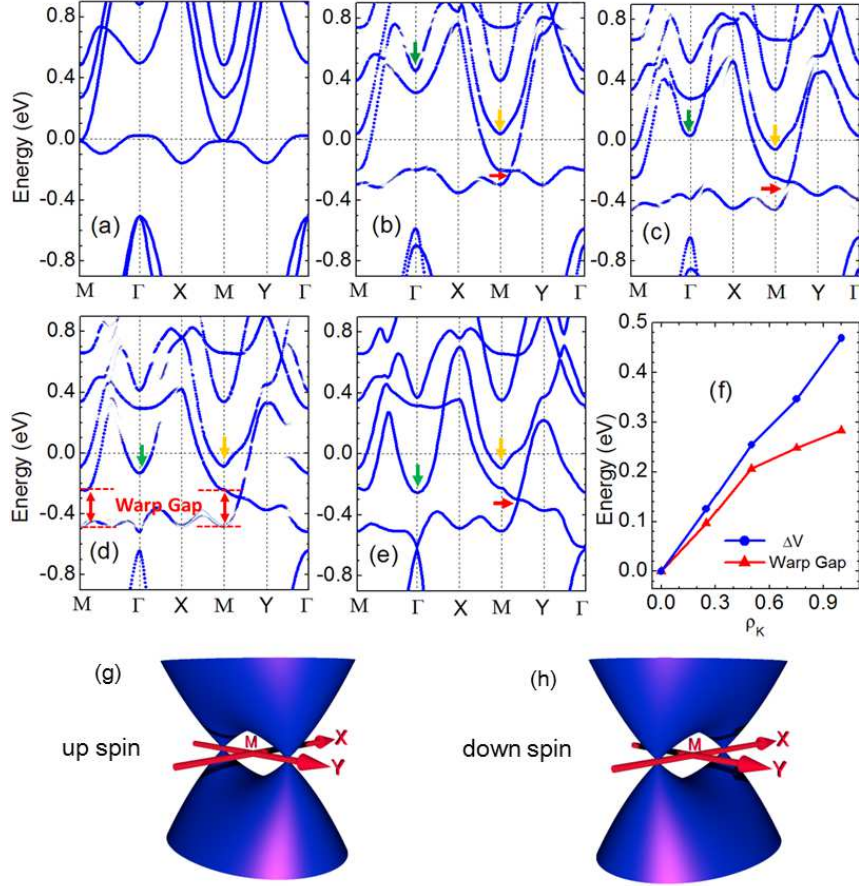


FIG. 3: (Color online) Spin-up unfolded electronic energy bands of checkerboard-AFM FeSe monolayer with $\rho_K = 0.25$ (b), 0.5 (c) and 0.75 (d). The spin-up electronic energy bands of FeSe primary cell with (e) and without (a) K atom adsorption are also shown here. Panel (f) shows the warp gap at M point and electric potential difference ΔV as functions of ρ_K . Panels (g) and (h) show the double-Weyl cones around M point for up and down spin electrons respectively.

strong electric field leads to an electric potential difference between top and bottom Se atoms ($\Delta V = V_{\text{top-Se}} - V_{\text{bot-Se}}$). The top (bottom) Se atoms are at the $\pm X$ ($\pm Y$) directions of a Fe atom with spin-up magnetic moment, and are at $\pm Y$ ($\pm X$) directions of a Fe atom with spin-down magnetic moment. Thus, ΔV will lead to a difference between X and Y directions. We studied the energy bands around the red arrow and find that they compose a double-Weyl cone structure. Different from Dirac cone, the Weyl cone does not have spin degeneracy. The sketches of double-Weyl cones for spin-up and spin-down electrons are shown in Figs. 3(g,h). The two Weyl points for up spin are in M-Y direction, while the two

Weyl points for down spin are in M-X direction. We name the energy gap at M point as a warp gap, as shown in Fig. 3(d). It characterizes the warping strength of energy bands. The calculated warp gap, as shown by the red line in Fig. 3(f), is found to linearly increase with the K coverage at the range of $0 < \rho_K < 0.5$. Its slope decreases when $\rho_K > 0.5$. We point out that such kinds of warp gaps have been observed in the 1-FeSe/SrTiO₃ system [7]. The fitted yellow line in Ref. [7] indicates the upper part of the double-Weyl cones in M- Γ direction in Fig. 1(b) of Ref. [7], wherein the bottom of the yellow line clearly departs from the lower energy bands. The estimated warp gap is about 50 meV. The warp gap can also be estimated from other ARPES experiments in 1-FeSe/SrTiO₃ system [25, 32]. From Figs. 2(b,c) in Ref. [32] and Fig. 2(d) in Ref. [25], we estimated that the warp gap is about 50 meV too. Based on our calculations, to observe the double-Weyl cone energy band structure, the ARPES spectra should be carried out along the M-X and M-Y directions. The ARPES spectrum would show four Weyl cones around M point both along M-X and M-Y directions, if the measurement does not distinguish the up and down electron spins. From previous studies [34], we know that the warp gap relates to ΔV directly. Thus, we calculated the value of ΔV too. The electronic potential at a Se atom was obtained by averaging the electronic potential at atom core area. The calculated ΔV is shown by the blue line in Fig. 3(f). It linearly depends on ρ_K in the whole K coverage range we considered.

The unfolded PCB K/FeSe energy bands are shown in Figs. 4(a-d). For $\rho_K = 0$ case, the unfolded energy bands in Fig. 4(a) show that there are double-Dirac cones around M point. It agrees with ARPES experiment results. Unlike the double-Weyl cones in CB FeSe, the double-Dirac cones in PCB FeSe exist without doping electrons. The connecting line between the two Dirac points is in Γ -M direction. They are the same for spin-up and spin-down electrons, as shown by the sketches in Figs. 4(e,f). The unfolding energy bands for $\rho_K = 0$ show that there is no Fermi surface exists at Γ point. The highest valence energy bands locates at about 100 meV below Fermi energy. This conflicts with ARPES experiments, which show the existence of hole-like Fermi pocket at Γ point. After K atom deposition ($\rho_K=0.25$), the whole energy bands move downwards with respect to Fermi energy. The Dirac points locates about 200 meV below Fermi energy. And the Fermi surfaces around M point combines to form a circle, as shown in Fig. 4(b). The PCB FeSe Fermi surface topology at $\rho_K=0.25$ is the same as that of CB FeSe. And it is consistent with ARPES experiment results. After we increase K atom coverage to $\rho_K=0.5$, an electron-like

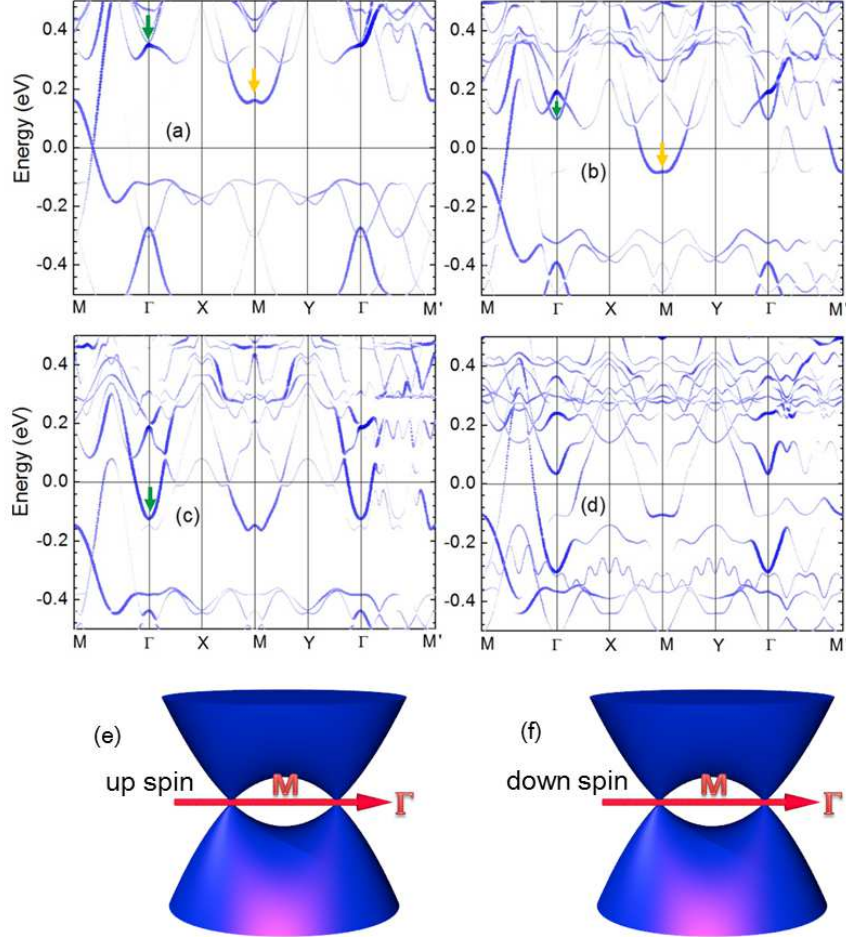


FIG. 4: (Color online) Spin-up unfolded electronic energy bands of PCB FeSe monolayer with $\rho_K = 0$ (a), 0.25 (b), 0.5 (c) and 0.75 (d). Panel (e) and (f) show the double-Dirac cones around M point for spin-up and spin-down electrons, respectively.

Fermi pocket exists at Γ point. It originates from the energy band bottom signed by a green arrow in Figs. 4(a-c). The energy band bottom crosses the Fermi level at $0.25 < \rho_K < 0.5$. The ρ_K at the crossing point is smaller than that in CB FeSe, which is $0.5 < \rho_K < 0.75$. As we further increase K atom coverage to $\rho_K=0.75$, the energy band bottom at Γ point lowers its energy, which increases the size of electron-like Fermi pocket.

From the energy band variations, we know that atomic K adsorption efficiently dopes electrons to the top FeSe layer. At this part, we examined the amount of doped electrons by performing Bader analysis [54]. In PCB FeSe, we used the $\sqrt{2} \times 2\sqrt{2}$ supercell models with 0~4 K atoms. The calculation results are shown in Fig. 5 by green blocks. In CB

FeSe, besides primary cell model for FeSe and K/FeSe, we also used three kinds of supercell models. They are 2×2 supercell with 1~3 K atoms, $\sqrt{5} \times \sqrt{5}$ supercell with 1~4 K atoms ($\rho_K = 0.2, 0.4, 0.6, 0.8$), and 3×3 supercell with 1 K atom ($\rho_K = \frac{1}{9}$). The Bader analysis results are shown in Fig. 5 by red down triangles. Besides the PCB and CB phases of FeSe monolayer, we also studied the K adsorption on paramagnetic phase (PM) of FeSe monolayer. The calculated electron transfer results are shown in Fig. 5 by up triangles. The electron transfers for PCB, CB and PM FeSe monolayers are the same for $\rho_K < 0.5$, and have a slight difference for $\rho_K \geq 0.6$. The maximum deviation is $0.016 e$, locating at $\rho_K = 0.75$. Thus, we conclude that the magnetic state of FeSe has negligible effect on the electron transfer from the adsorbed K atoms. The electron doping increases with increasing ρ_K . It is linear when $\rho_K < 0.5$. We fitted calculated data points (in unit of e) at this range by using $n_e = c \times \rho_K$. The n_e here is the amount of doped electrons per FeSe formula unit. The fitted slope c is 0.42. The value of n_e deviates from the $n_e = c \times \rho_K$ line for $\rho_K > 0.5$. It is lower than the linear line value. The knee point locates between $\rho_K = 0.5$ and 0.6 . It is near the place where Lifshitz transition may happen in PCB and CB FeSe layer.

The reported maximum value of electron transfer in experiment [40] is $0.15 e$. From the linear relation $n_e = c \times \rho_K$, we estimate that the ρ_K is about 0.36. It is still in the linear range. The corresponding CB FeSe energy band structure is in the interval between those shown in Figs. 3(b) and 3(c), where the electron pocket at Γ point still does not emerge. The PCB FeSe energy bands for $\rho_K = 0.36$ is in the interval between those shown in Figs. 4(b) and 4(c). It is the same interval where Lifshitz transition occurs. However, our linear extrapolation show that Lifshitz transition in PCB FeSe occurs at $\rho_K = 0.37$, which is larger than 0.36. Thus, electron pocket at Γ point does not emerge. Both the calculation results at PCB and CB FeSe are consistent with the ARPES experiment [40], which did not find any Fermi surface around Γ point. From the energy band structures in Figs. 3(a-e) and Figs. 4(a-c), and the linear relation $n_e = c \times \rho_K$, we estimate that the electron-like Fermi pocket at Γ point would appear for $n_e > 0.2 e$ in CB FeSe and $n_e > 0.17 e$ in PCB FeSe. To achieve this, the simplest way is to deposit more K atoms on top layer FeSe. To avoid the potential K-clustering problem sometimes occurred at large coverages, here, we propose an alternative experiment that can dope more electrons to FeSe monolayer. It is K deposition on monolayer FeSe grown on SrTiO_3 (001) surface. After sufficient annealing, SrTiO_3 substrate dope some amount of electrons to FeSe monolayer. Then the K deposition

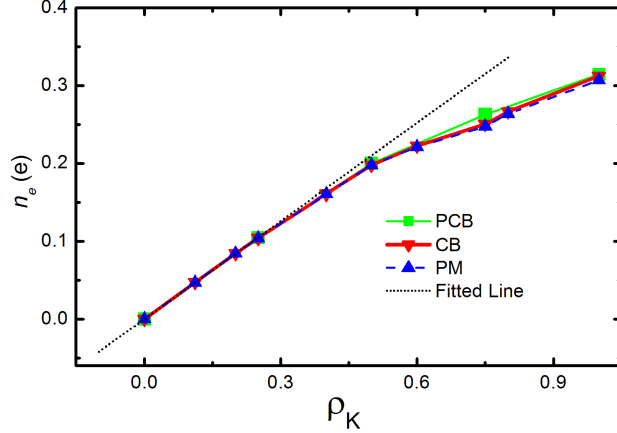


FIG. 5: (Color online) The charge doping (n_e) as a function of K atom coverage (ρ_K) in paramagnetic (green blocks), checkerboard-AFM (red down triangles), and pair-checkerboard-AFM (blue up triangles) FeSe. The dotted black line is fitted from small ρ_K data.

on FeSe monolayer will further increase the electron doping. The maximum n_e is probably larger than $0.2 e$. Interestingly, a previous experiment has already found an electron energy band centered at Γ point, existing 75 meV above Fermi energy [9]. It is very close to Fermi energy. The energy bands in this experiment would lie in the interval of Figs. 3(b) and 3(c), and is similar to Fig. 4(b). Thus, we estimate that once we dope more electrons to the system by K deposition, the Γ centered energy band would cross the Fermi level and introduce an additional electron-like Fermi pocket.

In summary, we have theoretically studied the atomic K deposition on n-FeSe/SrTiO₃ system. By using CB and PCB FeSe models, we explained the Fermi surface topology observed in experiment, i.e., the existence of electron-like pockets at M point, as well as the disappearance of the hole-like pockets and the enlargement of the electron-like pockets after K deposition. Our results show that the K adsorbate only affects the top layer FeSe. The charge transfer linearly depends on the K coverage in the range $0 < \rho_K < 0.5$ and leads to a strong electric field along the perpendicular direction of FeSe film. This strong electric field warps the CB FeSe energy band structure at M point and causes the occurrence of a double-Weyl cone structure. These Weyl points locate at M-Y and M-X high-symmetry lines for spin-up and spin-down electrons, respectively. Also, our energy band unfolding calculation shows that PCB FeSe contain double-Dirac cones at Fermi energy around M point for $\rho_K = 0$. They are along Γ -M direction. We have also shown that an electron-like Fermi pocket will

emerge at Γ point for $n_e > 0.2 e$ in CB FeSe and $n_e > 0.17 e$ in PCB FeSe, which is expected to be observed in the undergoing atomic K deposition experiments. Our obtained double-Weyl cones at M point and electron-like pocket at Γ point are typical features of CB FeSe. The spin-resolved experiments in the future will figure out whether CB or PCB magnetic orientation is the basement of the subsequent profound physics for the FeSe monolayer and thus increase our knowledge about this unique low-dimensional material.

This work was supported by Natural Science Foundation of China (NSFC) under Grant Nos. 11474030 and 91321103, and by the National Basic Research Program of China (973 Program) under Grant No. 2015CB921103.

-
- [1] Q.-Y. Wang *et al.*, Chin. Phys. Lett. **29**, 7402 (2012).
 - [2] D. Liu *et al.*, Nat. Commun. **3**, 931 (2012).
 - [3] S. Tan *et al.*, Nat. Mater. **12**, 634 (2013).
 - [4] J. He *et al.*, Proc. Natl. Acad. Sci. USA **111**, 18501 (2014).
 - [5] R. Peng *et al.*, Phys. Rev. Lett. **112**, 107001 (2014).
 - [6] R. Peng *et al.*, Nat. Commun. **5**, 5044 (2014).
 - [7] Y.-T. Cui *et al.*, Phys. Rev. Lett. **114**, 037002 (2015).
 - [8] Q. Fan *et al.*, arXiv:1504.02185.
 - [9] D. Huang *et al.*, arXiv:1503.04792.
 - [10] K. Liu, Z.-Y. Lu, and T. Xiang, Phys. Rev. B **85**, 235123 (2012).
 - [11] T. Bazhiron and M. L. Cohen, J. Phys. Condens. Matter **25**, 105506 (2013).
 - [12] R. Yuan, W. Kong, L. Yan, H. Ding, and N. Wang, Phys. Rev. B **87**, 144517 (2013).
 - [13] T. Berlijn *et al.*, Phys. Rev. B **89**, 020501 (2014).
 - [14] N. Hao and J. Hu, Phys. Rev. X **4**, 031053 (2014).
 - [15] H.-Y. Cao, S. Chen, H. Xiang, and X.-G. Gong, Phys. Rev. B **91**, 020504 (2015).
 - [16] K. Liu, B.-J. Zhang, and Z.-Y. Lu, Phys. Rev. B **91**, 045107 (2015).
 - [17] I. Mazin, Nat. Mater. **14**, 755 (2015).
 - [18] Y. Xie *et al.*, Sci. Rep. **5** (2015).
 - [19] S. Yang *et al.*, Nano Lett. **15**, 4150 (2015).
 - [20] M. Yi *et al.*, Nat. Commun. **6**, 7777 (2015).

- [21] L. Zhao *et al.*, arXiv:1505.06361.
- [22] J.-F. Ge *et al.*, Nat. Mater. **14**, 285 (2015).
- [23] Z. Zhang *et al.*, Science Bulletin **60**, 1301 (2015).
- [24] F.-C. Hsu *et al.*, Proc. Natl. Acad. Sci. USA **105**, 14262 (2008).
- [25] X. Liu *et al.*, Nat. Commun. **5** (2014).
- [26] L. Deng *et al.*, Phys. Rev. B **90**, 214513 (2014).
- [27] Q. Wang *et al.*, arXiv:1507.08431.
- [28] C.-L. Song *et al.*, Phys. Rev. B **84**, 020503 (2011).
- [29] F. Nabeshima, Y. Imai, M. Hanawa, I. Tsukada, and A. Maeda, Appl. Phys. Lett. **103**, 172602 (2013).
- [30] W. Zhang *et al.*, Phys. Rev. B **89**, 060506 (2014).
- [31] K. Shanavas and D. J. Singh, Phys. Rev. B **92**, 035144 (2015).
- [32] S. He *et al.*, Nat. Mater. **12**, 605 (2013).
- [33] J. Bang *et al.*, Phys. Rev. B **87**, 220503 (2013).
- [34] F. Zheng, Z. Wang, W. Kang, and P. Zhang, Sci. Rep. **3**, 2213 (2013).
- [35] Y.-Y. Xiang, F. Wang, D. Wang, Q.-H. Wang, and D.-H. Lee, Phys. Rev. B **86**, 134508 (2012).
- [36] B. Li, Z. Xing, G. Huang, and D. Xing, J. Appl. Phys. **115**, 193907 (2014).
- [37] J. Lee *et al.*, Nature **515**, 245 (2014).
- [38] S. Coh, M. L. Cohen, and S. G. Louie, New J. Phys. **17**, 073027 (2015).
- [39] L. Rademaker, Y. Wang, T. Berlijn, and S. Johnston, arXiv:1507.03967 .
- [40] Y. Miyata, K. Nakayama, K. Sugawara, T. Sato, and T. Takahashi, Nat. Mater. **14**, 775 (2015).
- [41] C. H. P. Wen *et al.*, arXiv:1508.05848.
- [42] C. Tang *et al.*, arXiv:1509.08950.
- [43] G. Kresse and J. Furthmüller, Comp. Mater. Sci. **6**, 15 (1996).
- [44] P. E. Blöchl, Phys. Rev. B **50**, 17953 (1994).
- [45] G. Kresse and D. Joubert, Phys. Rev. B **59**, 1758 (1999).
- [46] J. P. Perdew, K. Burke, and M. Ernzerhof, Phys. Rev. Lett. **77**, 3865 (1996).
- [47] J. Klimeš, D. R. Bowler, and A. Michaelides, Phys. Rev. B **83**, 195131 (2011).
- [48] P. Giannozzi *et al.*, J. Phys. Condens. Matter **21**, 395502 (2009).

- [49] D. Hamann, M. Schlüter, and C. Chiang, Phys. Rev. Lett. **43**, 1494 (1979).
- [50] J. J. Seo *et al.*, arXiv:1511.07950.
- [51] F. Zheng, P. Zhang, and W. Duan, Comput. Phys. Commun. **189**, 213 (2015).
- [52] A. A. Mostofi *et al.*, Comput. Phys. Commun. **178**, 685 (2008).
- [53] H. Huang *et al.*, New J. Phys. **16**, 033034 (2014).
- [54] G. Henkelman, A. Arnaldsson, and H. Jónsson, Comp. Mater. Sci. **36**, 354 (2006).